ADVANCED MATERIALS INTERFACES
Open Access
www.advmatinterfaces.de

Using Paper as a Biomimetic Fog Harvesting Material

Carina Breuer, Cynthia Cordt, Benjamin Hiller, Andreas Geissler, and Markus Biesalski**

This study identifies important factors for designing an effective biomimetic paper-based fog harvesting substrate by examining the harvesting properties of different surfaces, including glass, polyethylene, and superhydrophobic paper. In laboratory-scale fogging tests, the wetting behavior of the substrates is characterized, and the importance of the tilt angle of the respective surface relative to the fog flow is elaborated. Because successful fog harvesting requires both efficient accumulation of water droplets on the surface (by condensation and collision) and sufficient but not excessive roll-off of the liquid, the amount of water finally collected is clearly related to the pinning effect, which should prevent the smallest droplets from being carried away by the wind but must not lead to full and permanent wetting of the surface. Coalescence is identified as a major phenomenon to improve droplet roll-off. In this context, superhydrophobic paper indicates to be a more effective water collector than glass or polyethylene, especially when oriented vertically, since it allows the droplets to roll off very efficiently. Finally, the addition of glass particles to the superhydrophobic coating is proposed as a means of enhancing pinning and improving the fog harvesting efficiency.

1. Introduction

The collection of pure water from fog or humid air as an additional water resource has gained tremendous attention in recent years.[1] In 2002, the United Nations announced that "The human right to water is indispensable for leading a life in human dignity";[2] however, in 2022, 2.2 billion people still lacked safely managed drinking water.[3] Inhabitants of such areas are often forced to use water resources that are unhygienic and, furthermore, not easily accessible. Therefore, the amount of water per day is minimal, barely sufficient for cooking and drinking, without leaving much for hygiene or cultivation of food.[4–6] At present, water scarcity in these regions is particularly severe due to population growth, the expansion of agriculture, and rising industrial demand as well as increased drought periods caused by global warming.[4,7–11] This makes the availability of clean, reliable, economically feasible, and easy-to-operate water resources one of the greatest challenges in our century and especially important for developing countries in arid and semiarid regions. For this reason, especially compared to other recently developed fresh water collection strategies such as desalination, osmotic membrane, and sewage treatment, fog harvesting is the most promising way to alleviate water shortages.[11] Thus, since certain of these climatic areas have substantial amounts of fog, which accounts for up to 10% of all fresh water on earth,[12,13] fog collection has become a relevant alternative to alleviate shortages of water.[1,10,14]

For these reasons, fog collection has been investigated as a potential natural water source in arid or semiarid areas since the beginning of the 19th century.[1,4] As early as 1969, pioneering work was carried out in South Africa on the construction of an artificial fog collector. This fog collector consisted of two large plastic meshes with dimensions of 28 × 3.6m each and collected 31 m^3 water per month, that is, ≈11 L m^{-2} d^{-1}.[15] Due to the collision of fog droplets from the foggy wind passing through the mesh, followed by coalescence and formation of larger droplets, water flowed from the mesh via a gutter into a collecting channel.[4] Such early artificial fog collectors were made out of plastic meshes; however, to enhance the efficiency, a number of studies have been performed to modify the design of the fog collectors as well as the fog collecting materials themselves.[1]

Artificial fog harvesting materials can be nature-derived and are very often bioinspired by the structure and chemistry of animal or plant surfaces that are capable of collecting water from fog. Biological surfaces, for example, spider silk, cactus, Nepenthes, or Namib desert beetles, control the interaction with water using a variety of surface chemistry and morphological characteristics that enable water collection from the atmosphere even in arid environments.[1,8,16,17] They all share common heterogeneous surfaces with varying chemistry and topography, although the final water affinity is different.[7]

The backs of some Namib desert beetles, such as the prominent *Stenocara gracilipes* species, consist of bumpy regions with varying surface wettability. The structures were previously

C. Breuer, C. Cordt, A. Geissler, M. Biesalski
Macromolecular Chemistry and Paper Chemistry
Technical University of Darmstadt
Peter-Grünberg-Straße 8, 64287 Darmstadt, Germany
E-mail: andreas.geissler@tu-darmstadt.de;
markus.biesalski@tu-darmstadt.de

B. Hiller, A. Geissler
Papiertechnische Stiftung (PTS)
Pirnaer Str. 37, 01809 Heidenau, Germany

The ORCID identification number(s) for the author(s) of this article can be found under https://doi.org/10.1002/admi.202301048

DOI: 10.1002/admi.202301048

believed to be an arrangement of nonwaxy hydrophilic bumps ≈0.5 mm in diameter and 0.5–1.5 mm apart, surrounded by wax-coated hydrophobic regions.[18] Water from humid air and from fog that touches the beetle's back was believed to accumulate at the hydrophilic part and form droplets that increase continuously. Finally, the droplet would reach a critical size, and the surrounding areas with low water affinity would promote drainage from the beetle's back into its mouth once the growing droplets overcame capillary adhesion.[8,9,18] Later, however, this mechanism was challenged by Nørgaard et al.,[19] who found that the entire bumpy surface is covered with hydrophobic waxes. In addition to the varying surface wettability of the beetles back, recent studies highlight the role of the geometry of the convex millimeter-sized surface structures in condensation effects.[20–24] In addition to surface chemical and morphological properties that promote fog harvesting, some species of Namib desert beetle also exhibit special fog-basking behavior. For instance, beetles of the *Onymacris unguicularis* species turn their rumps upward into the fog-laden wind on dune crests in the early mornings, letting the fog deposit on their carapaces and the collected water roll down their body into the mouth.[19,25] Applying this behavior to artificial fog collectors implies that not only the material itself but also the substrate orientation into the fog is an important criterion.[26] Although the individual importance of different factors influencing the fog harvesting efficiency of Namib Desert beetles is still under discussion,[1,19,20] the hybrid wettability pattern has been proven to promote water collection out of fog by many hybrid wettability patterned artificial surfaces.[17]

Currently, researchers investigating such hybrid patterned surfaces focus on material development by mimicking the surface chemistry and morphology of natural models.[12,20,27,28] As reviewed by Sun et al.,[29] Wang et al.,[30] and Yu et al.,[31] several researchers have mimicked biosurfaces, such as spider silk,[32–34] cactus,[32,34–42] scallop shell,[43] or Namib desert beetle,[18,44–67] and multi-bioinspired approaches have also been used.[13,20,68–72] As in the approach presented here, various artificial fog harvesting surfaces are inspired by the Namib beetle. Therefore, a variety of approaches were investigated using different substrates, materials, and preparation methods, which, however, all have in common surface regimes of contrasting surface wettability as well as morphology, resulting in patterned water affinity, as in the natural model.

One common method is the deposition of hydrophilic structures in the order of micro- and nanoscales onto a (super)hydrophobic background, for instance, via spray coating of nanoparticles.[45,56,64] Another approach to achieve a contrast in wettability is a combination of hydrophobic microparticles with hydrophilic nanoparticles and induced formation of hierarchic structures by thermal treatment.[73] Instead of directly using particles with different wettabilities, particles with different reactivities toward silanes are applied to the surface and then functionalized to obtain hybrid wetting properties.[74,75] The creation of hydrophilic/hydrophobic patterns is also achieved by using masks combined with an etching or deposition process.[76,48] In addition to inorganic nanoparticles, polymers offer the possibility of creating domains with different wettabilities. For instance, polyelectrolytes or polymer solutions are applied on a superhydrophobic background using a pipet,[53,51] inkjet printing,[62] or plasma deposition.[52] Hydrophilic polymers are coated onto superhydrophobic substrates[53,52,61,77] and are then removed selectively using a laser to receive the hybrid surface.[47] Additionally, the dewetting behavior of hydrophilic polymer films on a hydrophobic polymer surface by thermal annealing is exploited to obtain hybrid wettability.[78,79] For these purposes, mainly inert substrates such as glass or silicon are used. Furthermore, cotton fabrics are also available as harvesting materials.[64,75,80–82] Interestingly, to date, no functional beetle-like paper substrates for water harvesting applications have been studied in detail, although paper is very similar to cotton fabrics among material resources. Yet, paper materials are used by Bai et al. forming cactus-inspired kirigami structures, whose geometry promote water collection.[35]

The physical process of collecting fog is highly complex and combines several factors whose individual relevance for fog collection efficiency has not been elucidated to date. The process of water collection consists of three fundamental steps: 1) moisture is transported toward the surface, 2) accumulates there, and 3) rolls off in a collection tank. The transport to the surface is dependent on the air circulation and its moisture content. The accumulation mechanism can be divided into two categories: collision and condensation. During collision, small air-suspended water droplets are carried to the surface by an air stream, collide on the surface and adhere to it. Most droplets are held regardless of the wettability of the surface due to the low inertia of the colliding drop and the adhesion between it and the surface.[83] Condensation can be described in three steps, that is, generation of supersaturation, formation of the droplet, and growth, which are dependent on the wettability of the surface as well as on the temperature. In general, hydrophilic surfaces exhibit lower energy barriers, which promote water condensation. In the case of fog collectors, collision has a higher impact on the collected amount of water compared to condensation.[84,85] Therefore, the wettability of the surface is of secondary importance. For the droplets draining off, the efficiency of water collection depends on the frequency as well as the mass of droplets during droplet removal.[86,87] This is influenced by the wetting regime, and the deposition of moisture can occur dropwise or filmwise. The latter is promoted by hydrophilic surfaces, while wetting becomes increasingly dropwise as the surface turns from hydrophobic to superhydrophobic. Filmwise wetting and thus completely hydrophilic surfaces are disadvantageous for water harvesting, as water drops have lower mobility, resulting in reduced drainage as the surface is covered and blocked for further water accumulation. In comparison, dropwise wetting, that is, on superhydrophobic surfaces, characterized by a small dynamic contact angle, results in efficient water roll-off and thereby increases the fog collection efficiency.[46,83,86] To combine the advantages of the better condensation behavior of hydrophilic surfaces with the superior roll-off behavior of superhydrophobic surfaces, hybrid surfaces, inspired by nature and outlined above, are very promising. In addition to increasing the condensation capacity, the introduction of hydrophilic spots on superhydrophobic backgrounds enables droplet pinning at the hydrophilic spots. This prevents the droplets from being carried away into the wind, which would reduce the collection efficiency.[86–89] In addition, small droplets can agglomerate at the hydrophilic spots to form larger droplets, which roll off the surface sooner due to their higher weight, increasing harvesting efficiency.[45]

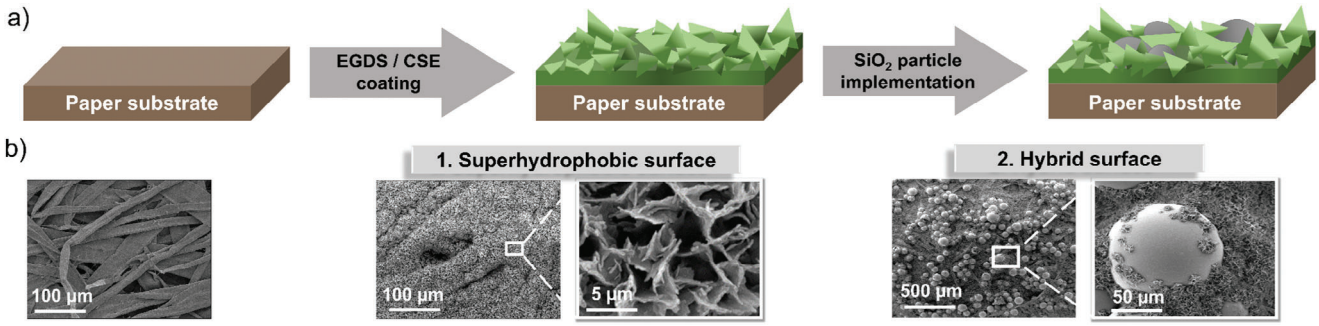

Figure 1. a,b) Schematic illustrations (a) and SEM images (b) of a native paper substrate followed by functionalization of this paper with a nanostructured superhydrophobic EGDS/CSE coating (1) and incorporation of spherical silica particles into this coating to achieve a hybrid wetting behavior (2).

Supplementing the many approaches on laboratory scale water-harvesting materials, our approach is specifically designed for a large-scale application as fog collector using paper as highly recyclable and additionally compostable material. Paper provides interesting properties for use as a substrate for water harvesting; however, it has not yet been developed for this application. Recently, we introduced functional paper materials in which the outer surfaces of paper fibers and sheets are modified with a superhydrophobic coating consisting of a nanostructured, semicrystalline polysaccharide-wax composite.[90] In this contribution, we extend this approach to turn water-repellent, superhydrophobic paper materials into efficient fog harvesting materials in a first step toward an entirely new design of fog collectors made of semifinished paper materials. Using paper instead of plastic meshes as a fog collector material is a great advantage, as paper is not only universally available and inexpensive but also a sustainable material that can be recycled or recovered after its lifetime on-site. In addition, our superhydrophobic approach using a water-based dispersion of bio-based cellulose polymers and waxes complements the advantages of paper as it can be applied with conventional paper machines on large scale while at the same time not interfering with the recycling of paper. We start by investigating the water harvesting properties of superhydrophobic wax-polymer–coated laboratory-made model papers based on ethylene glycol distearate (EGDS) and cellulose stearoyl ester (CSE) and then turn our focus to the water harvesting of hybrid coatings that contain regions of contrasting surface wettability adjacent to the superhydrophobic wax materials by implementing coating-embedded silica particles on the surface. To learn more about the mechanism of the fog collecting properties of our paper, we designed an apparatus in a climate-controlled chamber, where the collected water volume per surface area and time as well as the tilt angle of the substrate relative to the impact of the droplets from a fog machine can be varied and studied in detail.

2. Results and Discussion

The design and investigation of paper-based materials water harvesting are divided into two parts that are schematically shown in **Figure 1a**. In brief, the first part of this study focused on investigating the fog harvesting properties of a superhydrophobic paper coating based on EGDS and CSE in comparison to various model substrates. In the second part, the superhydrophobic surface coatings were transformed into surfaces with hybrid wettability by incorporating hydrophilic silica particles (Figure 1b), and the results were quantified and used to compare to the water harvesting capabilities of different models and the newly developed paper-based water harvesting devices.

With regard to the materials design, lab-made papers made from unbleached kraft pulp (UKP) were prepared and used. Due to the relatively long softwood fibers and the high degree of delignification, this pulp and the papers produced from it possessed high mechanical strength. To obtain superhydrophobic properties, the paper was treated with a previously developed superhydrophobic paper coating[90] consisting of a combination of a low-molecular–weight wax (EGDS) and a hydrophobic cellulose-based polymer (CSE). The polymer-wax composite formed well-defined nanoscale semicrystalline structures, as shown in Figure 1b. For details of the structure formation and investigations of the coating itself, we refer to our recent publications and to the Supporting Information (SI-1, Supporting Information) accompanying this contribution.

2.1. Fog Harvesting Mechanism and Properties of Superhydrophobic Paper Substrates

In the first step, the fog harvesting efficiency of a superhydrophobic paper with a rough waxy surface was compared with that of model substrates. As a hydrophilic reference with a smooth surface, a glass slide was selected, while polyethylene (PE) was chosen as a hydrophobic model substrate since it is a common material used for standard fog collector meshes. The wetting behavior of all samples was investigated by measuring their static and dynamic contact angles, which are shown in **Figure 2a**. The glass model substrate had a hydrophilic character with a static contact angle of 64° and a hysteresis of 45°, which indicated the strongest droplet pinning due to the interaction of water with hydroxyl groups of the surface. With a contact angle of 93° and a hysteresis of 22°, PE revealed a hydrophobic character due to its lower surface energy. The paper substrate was coated with an EGDS/CSE mixture with a mass ratio of 95/5 based on the work of Cordt et al.[90] as an aqueous dispersion. This resulted in wetting behavior in the superhydrophobic regime with a static contact angle close to 180° and a corresponding contact angle hysteresis of ≈0° resulting from its low surface energy combined with its surface roughness at the low micro scale.

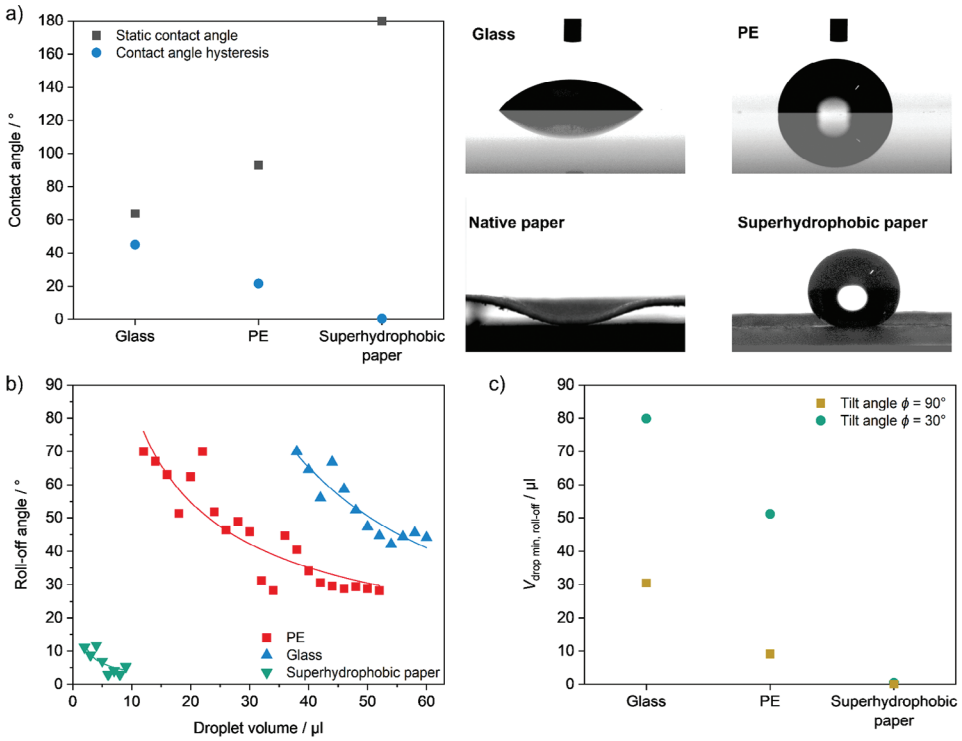

Figure 2. a–c) Wetting behavior of superhydrophobic paper substrate compared to PE and glass reference substrates: contact angles of water droplets (10 µL) sitting on surfaces (a), dependency between droplet volume and roll-off angle with allometric fit functions ($\gamma_{PE} = 372.19 \times x^{0.64}$, $\gamma_{glass} = 4423.76 \times x^{-1.14}$, $\gamma_{superh.\ paper} = 19.69 \times x^{-0.70}$) with coefficients of determination of $R^2_{PE} = 0.81$, $R^2_{glass} = 1.0$ and $R^2_{superh.\ paper} = 0.63$ (b), and from these fit functions calculated values for minimum water droplet volume for roll-off from the surfaces at tilt angles of 30° and 90° (c).

For efficient fog harvesting, the optimum between the adherence of the droplets to the surface and their roll-off is decisive, and the latter depends on the surface tilt and the size of the coalescing droplets. Therefore, the minimal droplet volume V_{drop} for rolling-off depending on the surface tilt angles ϕ (which corresponds to the roll-off angle during the contact angle measurement) was calculated by measuring the contact angle with varying droplet volume (Figure 2b).

The dependence of the necessary tilt angle on the droplet volume was obtained by an allometric fit function. The general allometric fit function with the variables a and b is given in Equation (1) and leads to the mathematical transformation for the needed droplet volumes for roll-off from surfaces with given orientations with $x = V$ and $y = \phi$ given in Equation (2). The equations with the values for the surfaces are given in SI-3 (Supporting Information).

$$\gamma_{surface} = a \times x^{-b}_{surface} \tag{1}$$

$$V_{drop,\ surface} = \left(\sqrt[b]{\phi_{surface} \times (a)^{-1}} \right)^{-1} \tag{2}$$

The resulting minimum drop volumes for different substrates with surface tilt angles of 30° or 90° are shown in Figure 2c. As already indicated by the results of contact angle measurements, the superhydrophobic paper exhibited the weakest droplet pinning, which results in even tiny droplets with volumes below 1 µL rolling off at a surface tilt angle of 30°. Glass, with a smooth and hydrophilic surface, exhibited the strongest pinning, resulting in relatively high droplet volumes of 30 and 80 µL rolling off at surface tilt angles of 90° and 30°, respectively. For PE, a smooth hydrophobic surface, the necessary droplet volume for roll-off was 9 µL at a 90° surface tilt angle and 51 µL at a 30° tilt angle.

The static contact angle measurements and the correlation with the roll-off needed droplet volumes showed a roll-off of minimal droplet volumes from the low-microstructured superhydrophobic paper compared to the smooth hydrophobic PE surface. Therefore, it was expected that the superhydrophobic paper would have a high fog harvesting efficiency due to the efficient roll-off behavior of the droplets, but at the same time, there was a risk that droplets would be swept away by the wind due to their low adhesion. The strong droplet adhesion on the smooth hydrophilic glass substrate compared to the superhydrophobic paper revealed this material to be optimal for water pinning areas to reduce droplet redeposition into the wind and promote droplet growth on the surface.

For measuring the fog harvesting properties of all three surfaces under controlled conditions (i.e., climate control), a laboratory setup was developed, as shown in SI-4 (Supporting Information) and schematically represented in **Figure 3a**, wherein the amount of water draining from the surface was measured gravimetrically. To observe the effects of droplet adhesion onto the surface and therefore the droplet roll-off efficiency, the fogging was processed with two different surface orientations: a tilt angle toward the fog stream of 90° and 30°. A linear regression of the water amount collected per time (see SI-5, Supporting Information,

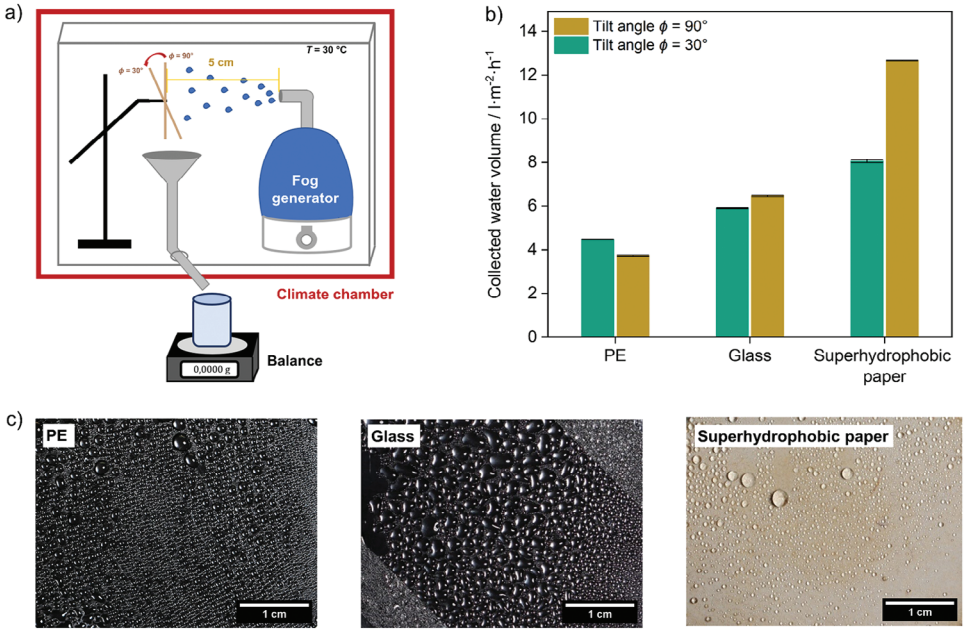

Figure 3. a–c) Schematic representation of the harvesting measurement setup (a), collected water volume per surface area and time at tilt angles of 30° and 90° (b), and photographs of wetted surfaces showing the different wetting properties (c).

for details) was used to calculate the fog collection rate expressed in water volume per time and surface area, which is shown for the three surfaces in Figure 3b. As one can infer from the data, the tilt angles of 30° and 90°, respectively, did not significantly influence water collection with glass or the PE substrate. However, for a superhydrophobic paper substrate, water collection at a tilt angle of 90° was almost twice the amount collected at a tilt angle of 30°. This difference can be explained by the excellent roll-off behavior of the surface, as discussed before. To enable a droplet to run off the surface, the droplet's gravitational force must overcome the capillary adhesion forces arising from the interaction with the surface. The capillary equation[86] (Equation (3)) gives the relationship between these two forces. The relevant parameters in this context are the density of water ρ_w, the gravitational constant g, the diameter of the contact area D_W, the surface energy of water γ, and the receding contact angle $\theta_{rec.}$

$$\rho_W \times g \times V_{drop} = \pi \times D_W \times \gamma \left(1 + \cos\theta_{rec}\right) \quad (3)$$

This equation shows the dependence of the gravitational force and therefore the droplet roll-off on the wettability of the substrate, given by the receding contact angle. Additionally, pictures of the befogged surfaces were taken and are shown in Figure 3c. The picture of the superhydrophobic paper surface indicates a dropwise wetting, where the water can run off the surface more efficiently than in filmwise wetting. In addition, heterogeneous condensation effects are expected to be more important for droplet growth, as dropwise condensation is known to be more than ten times more efficient than liquid film condensation.[91] For a tilt angle of 30°, the difference between the superhydrophobic surface and the reference surfaces in terms of the fog harvesting efficiency is small compared to that at 90°. However, the relative performance is still enhanced by 80%. The reason may be attributed to particularly small droplet volumes, which can move on the surface by convection forces, even against gravity, in low air fluxes, thus decreasing the total yield in the measurement setup. Therefore, we believe that a slight but not too strong pinning is advantageous, especially on single spots, to suppress filmwise wetting, as addressed in the second part of this work outlined below.

The hydrophilic glass slides, whose film-like surface wetting is shown in Figure 3c, can be regarded as the counterpart to the paper substrate in terms of wetting behavior. Filmwise wetting was shown to be inefficient for fog harvesting, which was consistent with the literature findings.[91] Once the surface was saturated, no further water could adhere to the surface, and the liquid was held strongly to the surface by interaction forces, which is referred to as pinning. This led to less efficient fog harvesting than on the superhydrophobic paper surface, but the results at a tilt angle of 90° were still better than for PE. According to the expectation resulting from previous contact angle measurements, the harvesting of hydrophobic PE should be larger because the droplet size needed for rolling off is smaller and surface wetting is dropwise. However, as shown in Figure 3c, more pronounced coalescence occurred on the glass surface, and the droplets grew faster. Due to this mechanism, the needed drop volume was exceeded more quickly with glass than with PE for a surface tilt of 90°. In addition, condensational effects can lead to higher harvesting. According to Volmer's classical nucleation theory, the free energy barrier for the formation of a liquid nucleus ΔG on a flat surface is defined via Equation (4) with the liquid–vapor surface energy σ_{lv} and the critical radius r^* and depends strongly on the wettability of the surface.[92]

$$\Delta G = \pi \sigma_{lv} r^{*2} \left(2 - 3\cos\theta + \cos^3\theta\right) \times 3^{-1} \quad (4)$$

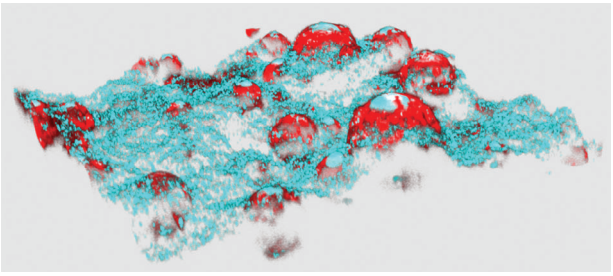

Figure 4. Confocal microscopy image of the paper coating with superhydrophobic waxes (blue) and implemented rhodamine B-stained glass particles (red).

This dependence shows that the nucleation energy barrier continuously increases with contact angle and is therefore larger for PE than for glass. PE had the least efficient harvesting abilities among the tested surfaces.

Overall, superhydrophobic paper at an orientation of 90° exhibited the highest efficiency of fog harvesting among the tested surfaces. The major advantage of the superhydrophobic paper surface and, according to our research, the decisive criteria for efficient water harvesting out of fog is the ability to remove water droplets from the surface more efficiently than the glass and PE surfaces, thus freeing the surface for further water adhesion. Moreover, this indicates that the effect of roll-off outweighs that of droplet accumulation. However, to further optimize the water-collecting tendency of the superhydrophobic surface, the advantages of effective dewetting of the superhydrophobic paper as well as the advantages of the glass surface (good accumulation and pinning to avoid droplet removal into the wind) are combined in a hybrid surface in the second part of this paper. Therefore, natural Namib desert beetle surfaces are mimicked by incorporating smooth glass particles as pinning centers in the superhydrophobic paper coating.

2.2. Improving Fog Harvesting Properties by Turning Superhydrophobic Papers into Hybrid Surfaces

In the second part of this study, a paper surface with hybrid wettability, as shown in Figure 1a (upper right scheme), was investigated. Smooth hydrophilic silica particles were incorporated by mixing them into the superhydrophobic dispersion, and scanning electron microscopy (SEM) analysis (Figure 1) as well as the confocal laser scanning microscopy (CLSM) analysis shown in **Figure 4** shows the embedding of the particles and the existence of smooth areas on the surface of the superhydrophobic paper coat. The smooth areas were created by the glass particles, which appear red in the confocal microscopy image due to staining with rhodamine B, whereas the reflection of the wax coating crystallites appears blue.

Based on the microscopy analysis alone, no insights can be gained into the surface energy of the incorporated particles and the hybrid surface. An important question was the amount of coverage of the particles by wax molecules during the coating process. In particular, it was important to know whether the particles were modified with a thin hydrophobic layer of wax. This was determined by a numerical approach based on contact angle measurements using the Cassie equation[93] (Equation (5)). According to this equation, the resulting contact angle θ of a heterogeneous surface can be calculated via the contact angles of the pure components θ_i and their respective surface fractions x_i.

$$\cos\theta = x_{\text{superh.surface}} \times \cos\theta_{\text{superh.surface}} + x_{\text{particle superh}} \times \cos\theta_{\text{particle superh}} \quad (5)$$

The wetting properties of the hydrophobic wax coating with suppressed crystallization were examined by the following procedure: The coating was applied on paper in the same manner as for the creation of superhydrophobic paper, but instead of cooling to room temperature under ambient conditions, the samples were quenched in liquid nitrogen from the molten state to suppress the crystallization process. The static contact angle of the quenched wax-coated paper was determined and compared to that of the superhydrophobic paper, as shown in **Figure 5a**. To gain insights into the pinning properties of these quenched samples (quenched coating (q.c.)), the roll-off angle was also determined (see Figure 5b). The quenched wax coating exhibited hydrophobic surface properties with a static contact angle of $\theta_{\text{q.c.}} = 102°$ and strong pinning properties compared to the superhydrophobic paper. This showed that even if the glass particles were covered with a thin hydrophobic wax layer, the wettability of the hybrid paper surface would be very heterogeneous due to the topographical effect alone.

The results of the Cassie equation are shown in Figure 5c,d. The curves indicate the dependency between the resulting contact angle of the hybrid paper and the respective contact angle of the glass beads. In this context, the red graph represents a surface fraction of 1% and the blue graph of 17% glass beads in the coating. The measured resulting contact angles of the substrates $\theta_{1\%}$ and $\theta_{17\%}$ are highlighted horizontally in the graph, with their errors considered. If the two options for the contact angles of the glass particles are used in the calculation, which can be 64° for pure glass (θ_{glass}) or 102° for wax-coated glass ($\theta_{\text{q.c.}}$), conclusions can be drawn by comparing the measured and theoretical data. For a fraction of 1%, there is no significant difference ($\Delta\theta$) in the calculated results using $\theta_{\text{glass}} = 64°$ and $\theta_{\text{q.c.}} = 102°$, especially considering the error of the measured value. For the substrate with a 17% surface fraction of glass beads, the difference between the measured and calculated values was much larger with $\Delta\theta_{\text{glass}} = 13°$ assuming uncovered glass particles than for covered hydrophobic glass particles with $\Delta\theta_{\text{q.c.}} = 1°$. This clearly indicated that the particles were covered by a thin layer of wax, which, according to the latest findings, also corresponds to the Namib desert beetle surface as a natural model.[17]

To investigate the influence of the pinning centers in more detail, hybrid surfaces with different SiO_2-particle coverages of ≈1% (0.75%) and ≈17% (17.32%) were prepared. The determination of the surface coverage with silica particles is described in SI-6 (Supporting Information). The wetting behavior and the fog harvesting properties of the hybrid paper surfaces were studied as before by contact angle measurements and laboratory fogging tests, respectively, and directly compared with those of plain wax-coated superhydrophobic paper as well as the reference material PE. **Figure 6a** shows the results of contact angle measurements. The incorporation of glass particles into the coating decreased the static contact angle from 180° to 169° for a particle surface

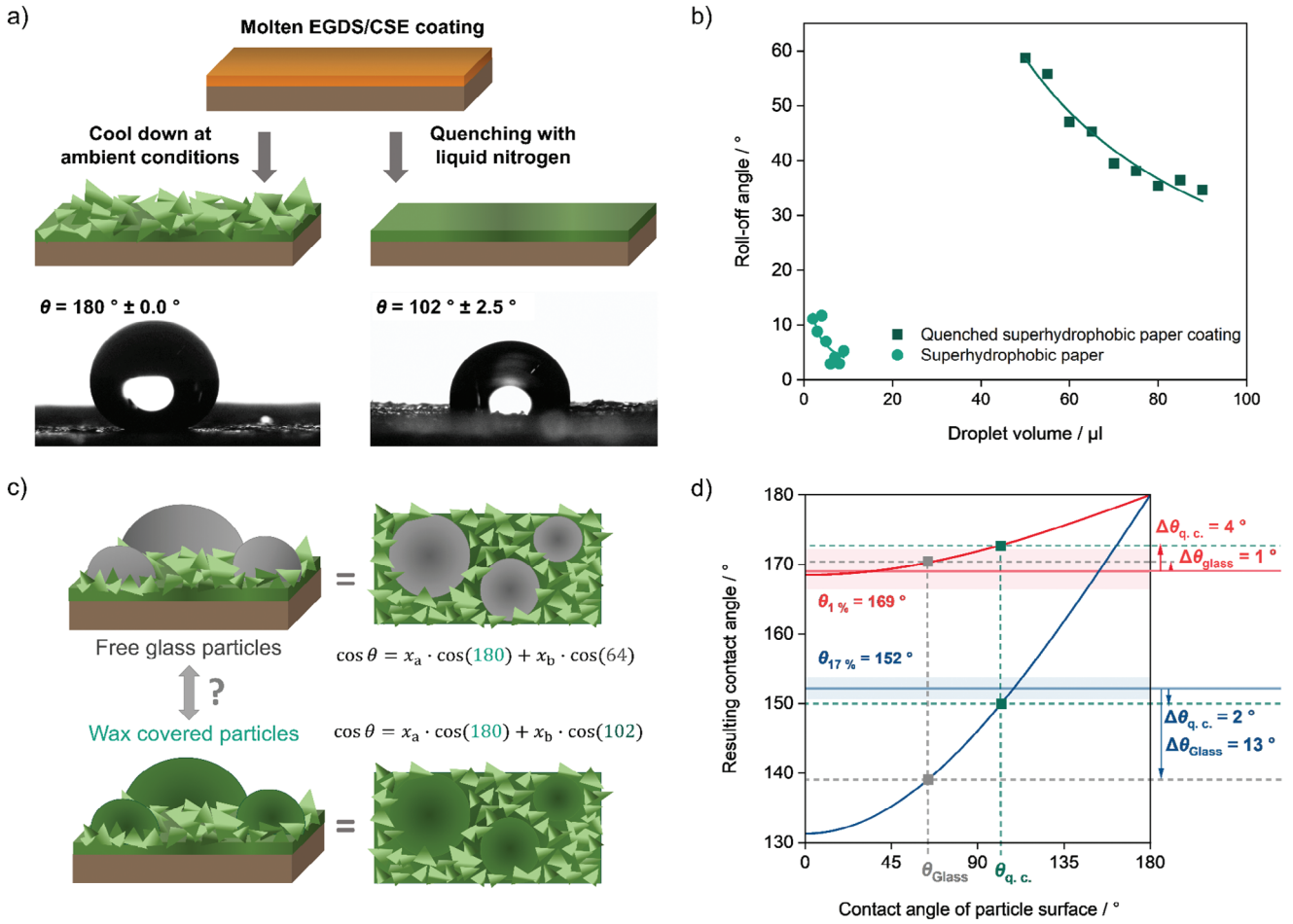

Figure 5. a) Schematic preparation path and static contact angle comparison of papers with crystallized and quenched (q.c.) CSE/EGDS coatings. b) Dependence between roll-off angle and droplet volume on these surfaces with allometric fit functions ($\gamma_{q.c.} = 2885.76 \times x^{1.00}$, $\gamma_{superh.\ paper} = 19.69 \times x^{0.70}$) with coefficients of determination of $R^2_{q.c.} = 0.96$ and $R^2_{superh.\ paper} = 0.63$. c,d) Schematic visualization of the question about wax-covered SiO_2 spheres (c) and mathematical approach with functions for resulting contact angles ($\gamma_{1\%} = \text{acos}\,(0.99 \times \cos(180) + 0.01 \times \cos(x))$, $\gamma_{17\%} = \text{acos}\,(0.83 \times \cos(180) + 0.17 \times \cos(x))$) and comparison of both models with real contact angles $\theta_{1\%} = 169°$ and $\theta_{17\%} = 152°$ (d).

coverage of 1% and further to 152° for a coverage of 17%. Additionally, the contact angle hysteresis increased with the addition of particles, which substantiates the pinning effects of the particles. The necessary minimum droplet volumes for roll-off from the surface at tilt angles of 30° and 90° are illustrated in Figure 6b and were obtained again by fit functions of the measurement of roll-off angles, shown in Figure 6c. In comparison to the superhydrophobic paper containing no silica particles, a different roll-off behavior was observed as a result of the particle implementation. The latter was expected to increase the efficiency of the fog collection. Whether this was achieved by the particle and whether low or high particle loading with consequently few or many pinning centers resulted in efficient fog harvesting was then investigated by performing laboratory fogging experiments. The original measurement data are shown in SI-7 (Supporting Information), and the results of the fog collection experiments carried out in comparison with polyethylene and superhydrophobic paper for surface tilt angles of 30° and 90° are shown in Figure 6d, respectively. As already discussed, the superhydrophobic paper performed 80% better than PE at a tilt of 30° and 240% better at a tilt of 90°, as the droplets rolled off more efficiently. The difference in the performance at 90° and 30° can be attributed to a potential loss of water because the air stream removes droplets from the surface, as discussed before. The latter interpretation was further supported by the low contact angle hysteresis, which showed a lack of pinning, as well as the minimum droplet volumes needed for the roll-off. By equipping superhydrophobic papers with hybrid wetting properties, the effectiveness of fog harvesting can even be improved. For a tilt angle of 90°, hybrid paper with a surface coverage of 1% SiO_2 particles can collect 8% more water than superhydrophobic paper, and for a surface tilt of 30°, the enhancement is 4%. The improvement can be explained by coalescence, which at least compensates for the potential deterioration due to the larger drop volume needed for roll-off. The coalescence leads to faster droplet growth and thus also to accelerated droplet roll-off, which is clear from the photographs in Figure 6e. As reported in the literature, coalescence is strongly affected by surface heterogeneity.[94] This makes the removal of water from the surface efficient, even though the droplet volume needed for roll-off is 1 to 5 µL larger than that for superhydrophobic paper.

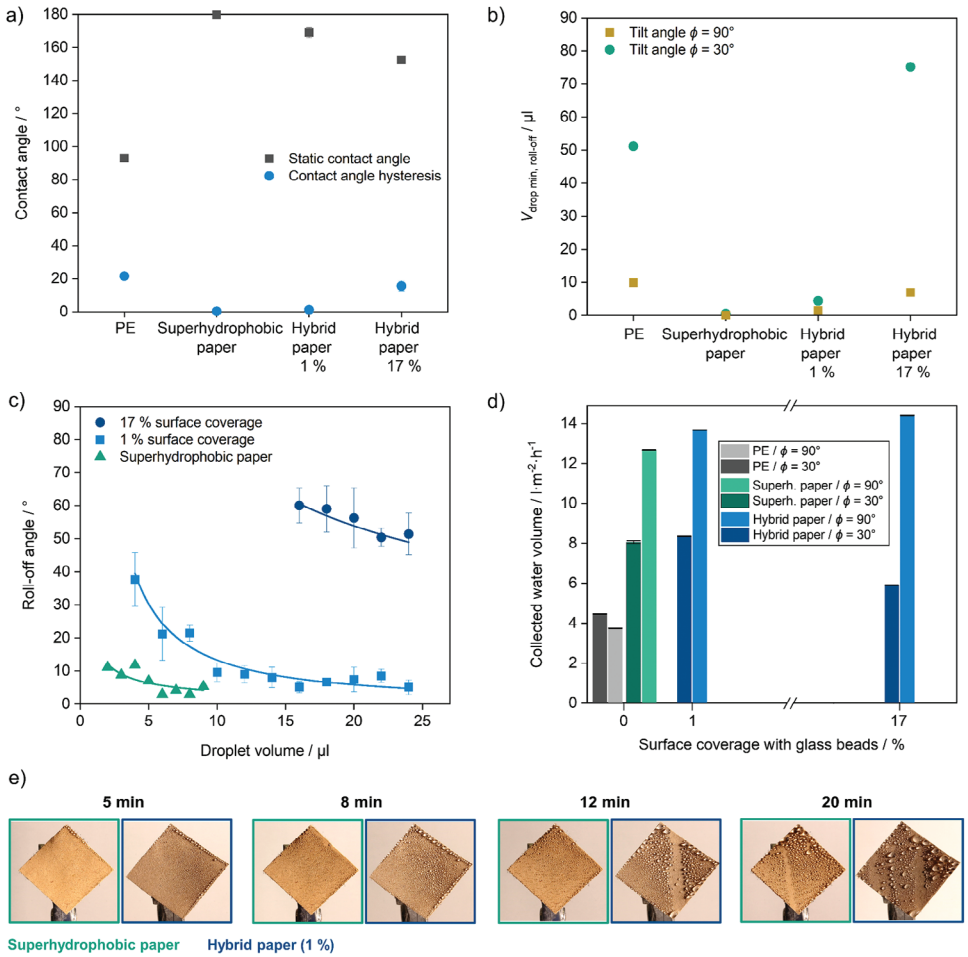

Figure 6. a–e) Wetting properties of the hybrid papers (a), droplet volumes needed for roll-off at the investigated tilt angles of 30° and 90° (b), roll-off angles for varied droplet volumes with allometric fit functions ($y_{17\%} = 259.80 \times x^{0.52}$, $y_{1\%} = 204.61 \times x^{1.19}$, $y_{superh.\ paper} = 19.69 \times x^{0.70}$) with coefficients of determination of $R^2_{17\%} = 0.89$, $R^2_{1\%} = 0.82$, and $R^2_{superh.\ paper} = 0.63$ (c), harvesting measurements of superhydrophobic papers without and with different amount of glass beads compared to a PE surface (d), and pictures of the befogging behavior of superhydrophobic paper versus (1% surface coverage) hybrid paper (e).

The small improvement in fog harvesting of 4% at a tilt angle of 30° can be attributed to coalescence and therefore a faster droplet growth speed; however, this effect is attenuated by stronger pinning. This is evident from the higher contact angle hysteresis and the larger drop volume needed for roll-off (Figure 6c). The fog droplets settle on the smooth domains on the substrate, which act as pinning centers; grow there, facilitated by coalescence; and finally roll down very efficiently because of the superhydrophobic background. At higher wind speeds, this protection mechanism caused by pinning could further improve harvesting efficiency due to the prevention of droplet loss in the fog stream and could strongly influence the harvesting efficiency for flat surface orientations. Looking at the hybrid papers with 17% particles on the surface, there was an increase in the collected amount of water of 14% for the surface tilt of 90° compared to the superhydrophobic paper but a decrease of 11% for the surface tilt of 30°. The droplet volume needed for roll-off at a 90° tilt angle was 7 µL higher than that for superhydrophobic paper, although this can be overcompensated in the vertical orientation by increased coalescence. At a surface tilt angle of 30°, the droplet volume needed for roll-off was almost 75 µL higher, which could no longer be compensated for by coalescence. The droplet pinning was too strong, reflecting the distinct influence of droplet roll-off on harvesting. As a result, these studies confirm that slight but not too strong pinning is important for optimal fog harvesting surface properties. In this context, the pinning zones provide local immobilization of the water droplets, but the adhesion forces, which depend on the surface coverage of these zones, should not be too high, so that the droplet roll-off remains efficient and can be compensated by coalescence. Likewise, the photos of the befogged paper substrates (Figure 6e) demonstrate the even more efficient fog collection of the hybrid compared to the superhydrophobic paper surface. It is evident that the smooth spots of the hybrid surface do not prevent dropwise wetting but rather cause faster growth of the droplets due to coalescence, allowing more water to adhere on the surface. Due to the faster droplet formation as well as increased volume, initial water drainage occurs at an earlier stage within the experimental setting (after 12 min for hybrid paper vs 20 min for superhydrophobic paper). This creates free areas for additional water accumulation, resulting in more efficient

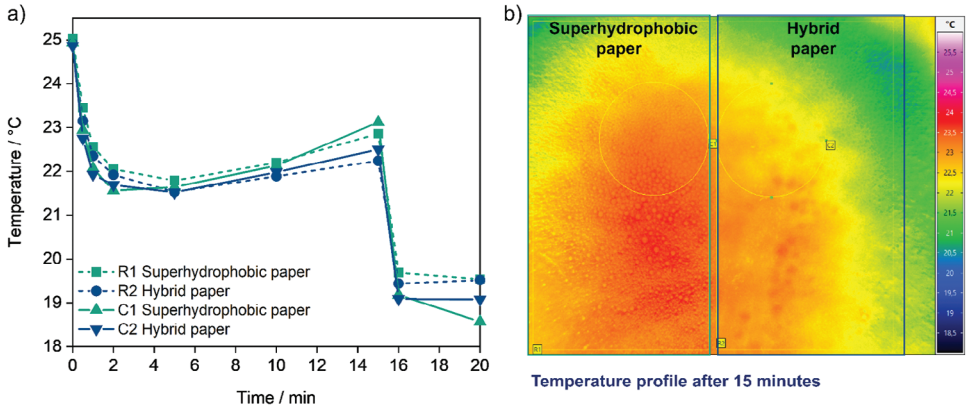

Figure 7. a,b) Surface temperature development, measured with a thermographic camera, of the superhydrophobic paper (green) and the hybrid paper (blue) during befogging (a) and the thermographic image of both samples after 15 min of befogging (b).

fog harvesting by faster droplet roll-off as well as larger draining droplets.

The wetting and fogging studies carried out revealed that, in addition to efficient drainage of the collected droplets, the process of water accumulation on the surface is also crucial. For the initial contact of water with the surface, two basic scenarios can be distinguished: collision and condensation. In the first case, droplets collide with the surface due to their kinetic energy and adhere there, while in the second case, the driving force is a temperature difference between the surface and the environment ($T_{surface} < T_{environment}$), which causes gaseous water to condense on the surface. The extent to which condensation effects contribute to water accumulation and thus fog harvesting is investigated by thermographic camera experiments with a high-performance photonic inspection system (**Figure 7**). For condensation, the temperature of the surface during fogging is critical. To identify a possible condensation-influencing effect of the SiO_2 particles in this context, a superhydrophobic surface and a hybrid surface with 1% particle coverage were monitored with a thermographic camera during fogging. The thermographic camera showed an overall cooler surface for the hybrid paper and cooler parts of the hybrid surface after 15 min, which could further enhance condensation. The decrease in temperature after 15 min of befogging in Figure 7a occurred due to evaporation effects. However, the absolute differences in temperature were rather low, and therefore so was the amount of condensation in the overall efficiency of water harvesting out of fog. Condensation plays a minor role compared to collision in water collection from fog, which already consists predominantly of small water droplets.

This supports our earlier hypothesis that fog harvesting on superhydrophobic paper is significantly improved compared to smooth hydrophilic and hydrophobic reference surfaces due to efficient droplet roll-off. Additionally, depending on the surface tilt angle, the water harvesting properties of superhydrophobic paper can be further improved by introducing water pinning centers. As the thermographic camera experiments demonstrate, a small proportion of the improvement is attributable to better accumulation of water due to condensation but a larger proportion to the pinning of water droplets, which prevents water from being lost into the wind and simultaneously promotes the nucleation of small water droplets into larger droplets that can overcome adhesion forces and roll off. However, the positive effect of pinning is limited, and should not be too high (as is the case on the plain glass model surface) and thus suppress efficient roll-off of the water into a collecting vessel.

Mechanistically, the efficient water collection with functionalized paper materials can be described as follows: Once small water particles transported by the fog stream are hitting the surface, water accumulates on the surface. Due to the low wettability of superhydrophobic surfaces, the water is forming spherical droplets, thus wetting the surface in a dropwise manner. During the ongoing fog stream, more water hits the surface, coalescing with the surface droplets and increasing their volume. Once the droplets reach a certain (surface specific) volume, the gravitational forces exceed the adhesion forces, whereas the drops roll off the surface and can be collected. Implementing areas with contrasting surface wettability, for example, without nanostructure, as in the case for the smooth spots on the hybrid paper surfaces, water droplets tend to pin at these areas resulting in coalescence of neighboring droplets at these areas thus leading to droplet growth. Due to the faster droplet growth relative to the superhydrophobic paper, the critical roll-off volume is reached earlier (even though it is higher for hybrid surfaces) and therefore more water can be collected at same time span.

3. Conclusion

In this work, the wetting behavior and fog harvesting ability of superhydrophobic paper substrates coated with a mixture of CSE and EGDS were examined. For comparison, a hydrophilic smooth glass substrate and a hydrophobic smooth PE substrate were investigated as model reference substrates. The coated paper material resulted in excellent water droplet roll-off behavior even for small tilt angles and droplet volumes due to the high static contact angle and very low contact angle hysteresis. The smooth reference surfaces possessed a stronger pinning effect for water droplets due to their lower static contact angle and correspondingly larger contact angle hysteresis. The experiments in this study demonstrated a correlation between surface wettability expressed by contact angles and the ability to harvest water out of fog. Efficient harvesting properties were observed for the superhydrophobic paper surface, especially for a tilt angle

of 90°. The fog droplets collided with the surface, grew on it, and rolled off with very high efficiency, which was highlighted as a key factor by the fog harvesting studies. For a small surface tilt of 30°, the harvesting was still more efficient than for the smooth model surfaces, but with a smaller difference. With a surface tilt angle of 30°, the loss of water droplets through air flow was much more pronounced than at 90°, which is why, in addition to efficient rolling, a certain pinning effect of the droplets is also beneficial. However, these are opposing effects that must be reconciled to find optimal surface properties. Therefore, superhydrophobic paper showing perfect roll-off is optimized for fog harvesting by implementing water pinning spots. For that purpose, smooth glass particles were incorporated onto the surface. As the fog harvesting experiments indicated, these smooth domains exhibited a pinning effect, but the whole surface still provided rapid water roll-off, resulting in efficient water collection. In addition to the protective mechanism of pinning, the particles further improved the efficiency of fog harvesting by coalescing the tiny water droplets on the spots, resulting in faster droplet growth and more efficient roll-off. Concurrently, the experiments showed a minor effect of condensation capabilities on the hybrid paper surface. However, with gaseous water collected from water vapor rather than from fog, which consists mainly of liquid water droplets, the relevance of the factors influencing the efficiencies may vary, which is the subject of ongoing research to extend the range of possible areas to introduce fog collectors.

While this study discovered that the optimal coverage of the superhydrophobic surface with pinning centers is between 1% and 17%, the optimal amount of water pinning centers influencing the roll-off behavior for different surface orientations to obtain the optimal harvesting capacity will be further investigated by varying the amount of silica particles. Therefore, the surface orientation is of great interest since hybrid paper surfaces provide great potential for use in paper-based fog collectors by incorporating such functionalized materials into different 3D and circular semifinished papers. Therefore, not only the paper surface itself but also the increased surface area promotes efficient water harvesting. Therefore, semifinished 3D water harvesting paper products in the form of honeycomb structures[95] can be used, in which the 3D structure can be easily used to adjust and enhance the fog collection rate. The incorporation of such surfaces into composite materials, for example, as lightweight constructs, is also conceivable.

4. Experimental Section

Materials: Demineralized water, ethylene glycol distearate (Carbosynth Ltd, United Kingdom, >85%, microcrystalline cellulose (Avicel, Sigma-Aldrich, 50 µm particle size), stearoyl chloride (>97%, TCI), toluene (99.85%, Thermo Scientific), pyridine (>99%, Carl Roth), ethanol (99.8%, Carl Roth), cationic starch (HI-CAT 21 370, Roquette), sorbitan monostearate (Span-60, synthesis grade, Sigma-Aldrich), glass bubbles (0.12 g cm^{-3}, white, R&G Faserverbundwerkstoffe), glass spheres (9–13 mm particle size, Sigma-Aldrich), rhodamine B isothiocyanate (mixed isomers, Sigma-Aldrich), 3-aminopropyl-dimethylethoxysilane (95%, Alfa Aesar). The paper material was pure UKP made from softwood without additives, basis weight of 100 g m^{-2}, produced on a pilot paper machine at PTS Heidenau.

Superhydrophobic Coating and Hybrid Surfaces: A 95:5 wt% mixture of EGDS (SI-1, Supporting Information) and CSE (SI-1, Supporting Information) was dispersed into water. In preparation, CSE with a degree of substitution (DS) of three was synthesized according to the literature:[90,96] 1 g of dried cellulose was suspended in 30 mL pyridine and heated to 100 °C. A total of 13.83 mL (6 mol per mol anhydroglucose units of cellulose) of stearoyl acid chloride was dropped into the suspension. The reaction was stirred at 100 °C for 1 h and poured into 200 mL of ethanol. The crude CSE was separated by centrifugation and purified through repeated boiling in ethanol. The slightly yellow product was dissolved in toluene and dried under vacuum. Yield: 5.60 g. Complete substitution (DS = 3) was confirmed by IR spectroscopy (SI-2, Supporting Information). To produce the aqueous dispersion with an EGDS/CSE content of 22 wt%, 23.75 g of EGDS and 1.25 g of CSE were premixed by stirring the molten substances at 85 °C for 4 h. Cationic starch (0.78 g, 3.18 wt%, related to EGDS) and sorbitan monostearate (0.5026 g, 1.17 mmol, 2.07 wt%, related to EGDS) were refluxed in 100 mL of water for 1 h. The hot EGDS/CSE mixture and the hot starch solution were poured together and mixed using an Ultra-Turrax at 20 000 rpm for 10 min (IKA, T 25 digital ULTRA-TURRAX®). Afterward, the dispersion was poured into a cooled beaker. The superhydrophobic dispersion was applied to 5 × 5 cm paper slices via dip coating using a velocity of 1 mm s^{-1}. If applicable, glass particles were added to the dispersion prior to coating. Therefore, 16.7 mg mL^{-1} glass spheres and 2.5 mg mL^{-1} glass bubbles were used. To obtain superhydrophobic properties, the coating was melted at 85 °C for 2 min and subsequently cooled under ambient conditions.

Smooth Hydrophobic Paper: The aqueous EGDS/CSE dispersion with a solid content of 22 wt% was applied onto paper via dip coating using a velocity of 1 mm s^{-1}. The paper was stored in an oven at 105 °C for 5 min to melt the coating. Immediately afterward, the paper was put into liquid nitrogen to suppress coating crystallization.

Labeling of Glass Particles with a Chromophore: According to the literature,[97] rhodamine B isothiocyanate (RITC) was functionalized with 3-aminopropyldimethylethoxysilane (APTMS). Therefore, 13.31 mg (7.42×10^{-5}, 10 eq.) APTMS and 4.00 mg (7.42 µmol, 1 eq.) RITC were refluxed in 7 mL dry ethanol for 1 h. The remaining solution was used without further purification and diluted with dry toluene to obtain a 0.01 wt% solution. The glass particles were placed in dry toluene and refluxed for 1 h after the addition of 0.1 mL dye solution g^{-1}. The glass particles were purified with toluene and ethanol.

Confocal Laser Scanning Microscopy: CLSM images were acquired using a Leica Microsystems TCS SP8 instrument with Leica Application Suite X software. The objective used was the HC PL APO CS2 (20×/NA0.75 DRY). Excitation was performed on three channels with λ_{EX} = 405, 488, and 552 nm. The detected wavelengths were λ_{EM} = 415–465 (autofluorescence of paper), 483–493 (reflection), and 565–610 nm (rhodamine B).

Fog Harvesting Measurements: For the measurement of the fog harvesting abilities, substrates of 5.0 × 5.0 cm were placed in a closed box (56.0 cm × 50.0 cm × 32.0 cm) in an oven at T = 30 °C (Memmert, UF160) and isolated from the surrounding temperature using a Styrofoam board (SI-4, Supporting Information). An ultrasonic humidifier (TaoTronics, T-AH002) with a volume stream of 3.8 mL min^{-1}) was used as the standard fog source, and substrates were befogged from a distance of 5 cm. The collected water was led out of the chamber via a glass bridge and dripped into a beaker. The collected amount of water was automatically measured with a balance (Adam, NBL 254i, software Adam DU). Each substrate was befogged for 1 h, and the fog harvesting efficiency expressed in water weight per time was calculated via the slope of the linear relation of the water weight per time and surface area whereas the error of collected water results is based on the slope error of linear regression.

Contact Angle Measurement: Static contact angles were measured with a contact angle device OCA35 from Dataphysics under standard climate conditions (23 °C, 50% RH) with a 10 µL ultrapure water droplet (Milli-Q, Advantage A10, Millipak Express 20, Merck Millipore) and fitted with the Young–Laplace model. At least five droplets were measured for each surface, and an average value was determined, whereby the error represents the standard error of the mean, which is the standard deviation divided by the square root of the sample size. For dynamic contact angle measurements, the tilt unit TBU 90E from Dataphysics was used, and the analysis of drop shape was performed by elliptical fit. Via these

measurements, contact angle hysteresis was obtained by calculation using the advancing and receding contact angle of the drop immediately before roll-off.

Scanning Electron Microscopy: The samples were sputtered with 10 nm Pt/Pd (80/20) in argon plasma using a Sputter Coater 208 HR from Cressington. An SEM Type XL 30 from Philips equipped with a field emission gun and a secondary electron detector with an acceleration voltage of 5 or 10 keV were used.

Thermal Camera: For comparison of temperatures of a superhydrophobic paper and a hybrid paper during befogging, a photonic high-performance inspection system XGA was used. The camera contained a self-cooling measurement system to reduce the influence of the camera's self-heating on the measurement result by means of a Stirling rotary cooler. The detector format was 1.280 × 1.024 infrared pixels. The high thermal resolution was in the range of <30 mK, and the frame rate was 180 Hz in the full frame (up to 2601 Hz online) due to the low integration time (exposure time) of the camera. A sample half coated with a superhydrophobic coating and half with a hybrid coating was befogged with an ultrasonic humidifier (TaoTronics, T-AH002) with a volume stream of 7.2 mL min^{-1}) for 15 min, and the temperature of the surface was measured after 0.5, 1, 2, 5, 10, and 15 min as well as 1 and 5 min after the end of befogging at room temperature.

Supporting Information

Supporting Information is available from the Wiley Online Library or from the author.

Acknowledgements

C.B. and C.C. contributed equally to this work. The authors gratefully acknowledge the support of Steffen Schramm (PTS Heidenau) for the production of paper at the pilot plant and the support of Tobias Meckel (TU Darmstadt) with confocal imaging. The authors further kindly acknowledge the financial support through the Collaborative Research Center 1194 "Interaction of Transport and Wetting Processes," Project A05, funded by the Deutsche Forschungsgemeinschaft (DFG, German Research Foundation) – Project-ID 265191195—SFB 1194. Likewise, the authors would like to acknowledge the support of the German Federal Ministry for Economic Affairs and Climate Action within the funding program "FuE-Förderung gemeinnütziger externer Industrieforschungseinrichtungen in Ostdeutschland—Innovationskompetenz Ost" (INNO-KOM-OST), Project-ID 49IZ200010.

Open access funding enabled and organized by Projekt DEAL.

Conflict of Interest

The authors declare no conflict of interest.

Data Availability Statement

The data that support the findings of this study are available in the supplementary material of this article.

Keywords

biomimetic surface, droplet pinning, fog harvesting, paper materials, paper wetting, superhydrophobic wetting, water harvesting

Received: December 19, 2023
Published online: January 14, 2024

[1] M. Azeem, M. T. Noman, J. Wiener, M. Petru, P. Louda, *Environ. Technol. Innovation* **2020**, *20*, 101169.
[2] United Nations, committee on economic, social and cultural rights, The right to water, https://www.refworld.org/docid/4538838d11.html (accessed: June 2023).
[3] United Nations Children's Fund (UNICEF) and World Health Organization (WHO), https://cdn.who.int/media/docs/default-source/wash-documents/jmp-2023_layout_v3launch_5july_low-reswhowebsite.pdf?sfvrsn=c52136f5_3&download=true (accessed: October 2023).
[4] M. Fessehaye, S. A. Abdul-Wahab, M. J. Savage, T. Kohler, T. Gherezghiher, H. Hurni, *Renewable Sustainable Energy Rev.* **2014**, *29*, 52.
[5] O. Klemm, R. S. Schemenauer, A. Lummerich, P. Cereceda, V. Marzol, D. Corell, J. Van Heerden, D. Reinhard, T. Gherezghiher, J. Olivier, P. Osses, J. Sarsour, E. Frost, M. J. Estrela, J. A. Valiente, G. M. Fessehaye, *Ambio* **2012**, *41*, 221.
[6] A. F. Batisha, *Sustainability Water Qual. Ecol.* **2015**, *6*, 1.
[7] P. S. Brown, B. Bhushan, *Phil. Trans. R. Soc. A* **2016**, *374*, 20160135.
[8] S. Zhang, J. Huang, Z. Chen, Y. Lai, *Small* **2017**, *13*, 1602992.
[9] K. Wan, X. Gou, Z. Guo, *J Bionic Eng.* **2021**, *18*, 501.
[10] M. Qadir, G. Jiménez, R. Farnum, L. Dodson, V. Smakhtin, *Water* **2018**, *10*, 372.
[11] K. Zhang, H. Chen, T. Ran, L. Zhang, Y. Zhang, D. Chen, Y. Wang, Y. Guo, G. Liu, *ACS Appl. Mater. Interfaces* **2022**, *14*, 33993.
[12] Y. Su, L. Chen, Y. Jiao, J. Zhang, C. Li, Y. Zhang, Y. Zhang, *ACS Appl. Mater. Interfaces* **2021**, *13*, 26542.
[13] X. Wang, Z. Guo, W. Liu, *Adv. Mater. Interfaces* **2023**, *10*, 2202123.
[14] S. Korkmaz, I. A. Kariper, *Environ. Chem. Lett.* **2020**, *18*, 361.
[15] J. Olivier, *Water* **2002**, *28*, 349.
[16] J. R. Henschel, M. K. Seely, *Atmos. Res.* **2008**, *87*, 362.
[17] G. He, C. Zhang, Z. Dong, *iScience* **2023**, *26*, 105819.
[18] A. R. Parker, C. R. Lawrence, *Nature* **2001**, *2001*, 33.
[19] T. Nørgaard, M. Dacke, *Front Zool.* **2010**, *7*, 23.
[20] K.-C. Park, P. Kim, A. Grinthal, N. He, D. Fox, J. C. Weaver, J. Aizenberg, *Nature* **2016**, *531*, 78.
[21] J. L. Viovy, D. Beysens, C. M. Knobler, *Phys. Rev. A.* **1988**, *37*, 4965.
[22] A. Shahrokhian, J. Feng, H. King, *J R Soc Interface* **2020**, *17*, 20200038.
[23] B.-E. Pinchasik, M. Kappl, H.-J. Butt, *ACS Nano* **2016**, *10*, 10627.
[24] M. A. K. Azad, D. Ellerbrok, W. Barthlott, K. Koch, *Bioinspir. Biomim.* **2015**, *10*, 016004.
[25] W. J. Hamilton, M. K. Seely, *Nature* **1976**, *1976*, 284.
[26] B. Khalil, J. Adamowski, A. Shabbir, C. Jang, M. Rojas, K. Reilly, B. Ozga-Zielinski, *Sustain Water Resour Manag* **2016**, *2*, 71.
[27] Y. Xing, W. Shang, Q. Wang, S. Feng, Y. Hou, Y. Zheng, *ACS Appl. Mater. Interfaces* **2019**, *11*, 10951.
[28] L. T. Nguyen, Z. Bai, J. Zhu, C. Gao, X. Liu, B. T. Wagaye, J. Li, B. Zhang, J. Guo, *ACS Omega* **2021**, *6*, 3910.
[29] H. Sun, Y. Song, B. Zhang, Y. Huan, C. Jiang, H. Liu, T. Bao, S. Yu, H. Wang, *Appl. Phys. A.* **2021**, *127*, 461.
[30] Q. Wang, F. Yang, Z. Guo, *J. Mater. Chem. A.* **2021**, *9*, 22729.
[31] Z. Yu, T. Zhu, J. Zhang, M. Ge, S. Fu, Y. Lai, *Adv. Funct. Mater.* **2022**, *32*, 2200359.
[32] T. Xu, Y. Lin, M. Zhang, W. Shi, Y. Zheng, *ACS Nano* **2016**, *10*, 10681.
[33] Y. Zheng, H. Bai, Z. Huang, X. Tian, F.-Q. Nie, Y. Zhao, J. Zhai, L. Jiang, *Nature* **2010**, *463*, 640.
[34] J. Ju, Y. Zheng, L. Jiang, *Acc. Chem. Res.* **2014**, *47*, 2342.
[35] H. Bai, T. Zhao, X. Wang, Y. Wu, K. Li, C. Yu, L. Jiang, M. Cao, *J. Mater. Chem. A.* **2020**, *8*, 13452.
[36] J. Ju, K. Xiao, X. Yao, H. Bai, L. Jiang, *Adv. Mater.* **2013**, *25*, 5937.
[37] J. Ju, X. Yao, S. Yang, L. Wang, R. Sun, Y. He, L. Jiang, *Adv. Funct. Mater.* **2014**, *24*, 6933.
[38] H. Bai, C. Zhang, Z. Long, H. Geng, T. Ba, Y. Fan, C. Yu, K. Li, M. Cao, L. Jiang, *J. Mater. Chem. A.* **2018**, *6*, 20966.

[39] X. Li, Y. Yang, L. Liu, Y. Chen, M. Chu, H. Sun, W. Shan, Y. Chen, *Adv. Mater. Interfaces* **2019**, *7*, 1901752.
[40] S. Yi, J. Wang, Z. Chen, B. Liu, L. Ren, L. Liang, L. Jiang, *Adv. Mater. Technol.* **2019**, *4*, 1900727.
[41] M. Cao, J. Ju, K. Li, S. Dou, K. Liu, L. Jiang, *Adv. Funct. Mater.* **2014**, *24*, 3235.
[42] J. Ju, X. Yao, S. Yang, L. Wang, R. Sun, Y. He, L. Jiang, *Adv. Funct. Mater.* **2014**, *24*, 6933.
[43] H. Bai, X. Wang, Z. Li, H. Wen, Y. Yang, M. Li, M. Cao, *Adv. Mater.* **2023**, *35*, 2211596.
[44] C. Wen, H. Guo, H. Bai, T. Xu, M. Liu, J. Yang, Y. Zhu, W. Zhao, J. Zhang, M. Cao, L. Zhang, *ACS Appl. Mater. Interfaces* **2019**, *11*, 34330.
[45] X. Wang, J. Zeng, X. Yu, Y. Zhang, *J. Mater. Chem. A.* **2019**, *7*, 5426.
[46] Y. Hou, M. Yu, X. Chen, Z. Wang, S. Yao, *ACS Nano* **2015**, *9*, 71.
[47] E. Kostal, S. Stroj, S. Kasemann, V. Matylitsky, M. Domke, *Langmuir* **2018**, *34*, 2933.
[48] Z. Yu, F. F. Yun, Y. Wang, L. Yao, S. Dou, K. Liu, L. Jiang, X. Wang, *Small* **2017**, *13*, 1701403.
[49] L. Zhong, H. Zhu, Y. Wu, Z. Guo, *J. Colloid Interface Sci.* **2018**, *525*, 234.
[50] H. Zhu, R. Duan, X. Wang, J. Yang, J. Wang, Y. Huang, F. Xia, *Nanoscale* **2018**, *10*, 13045.
[51] C. Dorrer, J. Rühe, *Langmuir* **2008**, *24*, 6154.
[52] R. P. Garrod, L. G. Harris, W. C. E. Schofield, J. Mcgettrick, L. J. Ward, D. O. H. Teare, J. P. S. Badyal, *Langmuir* **2007**, *23*, 689.
[53] L. Zhai, M. C. Berg, F. Ç. Cebeci, Y. Kim, J. M. Milwid, M. F. Rubner, R. E. Cohen, *Nano Lett.* **2006**, *6*, 1213.
[54] X. Yang, J. Song, J. Liu, X. Liu, Z. Jin, *Sci. Rep.* **2017**, *7*, 8816.
[55] C. Xu, R. Feng, F. Song, X.-L. Wang, Y.-Z. Wang, *ACS Sustainable Chem. Eng.* **2018**, *6*, 14679.
[56] W. Huang, X. Tang, Z. Qiu, W. Zhu, Y. Wang, Y.-L. Zhu, Z. Xiao, H. Wang, D. Liang, J. Li, Y. Xie, *ACS Appl. Mater. Interfaces* **2020**, *12*, 40968.
[57] R. Zhu, M. Liu, Y. Hou, L. Zhang, M. Li, D. Wang, D. Wang, S. Fu, *ACS Appl. Mater. Interfaces* **2020**, *12*, 50113.
[58] M. Gürsoy, *Colloid Polym. Sci.* **2020**, *298*, 969.
[59] K. Yin, H. Du, X. Dong, C. Wang, J.-A. Duan, J. He, *Nanoscale* **2017**, *9*, 14620.
[60] J. Park, S. Kim, *Micromachines* **2019**, *10*, 201.
[61] Y. Wang, L. Zhang, J. Wu, M. N. Hedhili, P. Wang, *J. Mater. Chem. A.* **2015**, *3*, 18963.
[62] L. Zhang, J. Wu, M. N. Hedhili, X. Yang, P. Wang, *J. Mater. Chem. A.* **2015**, *3*, 2844.
[63] I. A. Kariper, *npj Clean Water* **2021**, *4*, 24.
[64] Y. Wang, X. Wang, C. Lai, H. Hu, Y. Kong, B. Fei, J. H. Xin, *ACS Appl. Mater. Interfaces* **2016**, *8*, 2950.
[65] Y. Gao, J. Wang, W. Xia, X. Mou, Z. Cai, *ACS Sustainable Chem. Eng.* **2018**, *6*, 7216.
[66] Y.-Y. Song, Y. Liu, H.-B. Jiang, S.-Y. Li, C. Kaya, T. Stegmaier, Z.-W. Han, L.-Q. Ren, *Nanoscale* **2018**, *10*, 16127.
[67] B. White, A. Sarkar, A.-M. Kietzig, *Appl. Surf. Sci.* **2013**, *284*, 826.
[68] S. Zhang, M. Chi, J. Mo, T. Liu, Y. Liu, Q. Fu, J. Wang, B. Luo, Y. Qin, S. Wang, S. Nie, *Nat. Commun.* **2022**, *13*, 4168.
[69] D. Chen, J. Li, J. Zhao, J. Guo, S. Zhang, T. A. Sherazi, Ambreen, S. Li, *J. Colloid Interface Sci.* **2018**, *530*, 274.
[70] Z. Yu, J. Zhang, S. Li, Z. Zhou, Z. Qin, H. Liu, Y. Lai, S. Fu, *Adv. Funct. Mater.* **2023**, *33*, 2210730.
[71] Y. Zhang, F. Wang, Y. Yu, J. Wu, Y. Cai, J. Shi, H. Morikawa, C. Zhu, *Chem. Eng. J.* **2023**, *466*, 143330.
[72] H. Venkatesan, J. Chen, H. Liu, W. Liu, J. Hu, *Adv. Funct. Mater.* **2020**, *30*, 2002437.
[73] J. Feng, L. Zhong, Z. Guo, *Chem. Eng. J.* **2020**, *388*, 124283.
[74] X. Wang, J. Zeng, X. Yu, C. Liang, Y. Zhang, *Appl. Surf. Sci.* **2019**, *465*, 986.
[75] B. Wang, Y. Zhang, W. Liang, G. Wang, Z. Guo, W. Liu, *J. Mater. Chem. A.* **2014**, *2*, 7845.
[76] J. Wu, L. Zhang, Y. Wang, P. Wang, *Adv. Mater. Interfaces* **2017**, *4*, 1600801.
[77] B. Mondal, M. M. G. Eain, Q. Xu, V. M. Egan, J. Punch, A. M. Lyons, *ACS Appl. Mater. Interfaces* **2015**, *7*, 23575.
[78] S. C. Thickett, C. Neto, A. T. Harris, *Adv. Mater.* **2011**, *23*, 3718.
[79] I. Wong, G. H. Teo, C. Neto, S. C. Thickett, *ACS Appl. Mater. Interfaces* **2015**, *7*, 21562.
[80] H. Yang, H. Zhu, M. M. R. M. Hendrix, N. J. H. G. M. Lousberg, G. De With, A. C. C. Esteves, J. H. Xin, *Adv. Mater.* **2013**, *25*, 1149.
[81] J. Ter Schiphorst, M. Van Den Broek, T. De Koning, J. N. Murphy, A. P. H. J. Schenning, A. C. C. Esteves, *J. Mater. Chem. A.* **2016**, *4*, 8676.
[82] M. Cao, J. Xiao, C. Yu, K. Li, L. Jiang, *Small* **2015**, *11*, 4379.
[83] Y. Jiang, C.-H. Choi, *Adv. Mater. Interfaces* **2021**, *8*, 2001205.
[84] S. Heidenreich, *Chem. Ing. Tech.* **2005**, *77*, 35.
[85] N. H. Fletcher, *J. Chem. Phys.* **1958**, *29*, 572.
[86] D. Seo, J. Lee, C. Lee, Y. Nam, *Sci. Rep.* **2016**, *6*, 24276.
[87] S. Choo, H.-J. Choi, H. Lee, *Appl. Surf. Sci.* **2015**, *324*, 563.
[88] V. S. Nikolayev, D. Beysens, A. Gioda, I. Milimouka, E. Katiushin, J.-P. Morel, *J. Hydrol.* **1996**, *182*, 19.
[89] J. D. D. Rivera, *Atmos. Res.* **2011**, *102*, 335.
[90] C. Cordt, A. Geissler, M. Biesalski, *Adv. Mater. Interfaces* **2021**, *8*, 2001265.
[91] H. Luo, Y. Lu, S. Yin, S. Huang, J. Song, F. Chen, F. Chen, C. J. Carmalt, I. P. Parkin, *J. Mater. Chem. A.* **2018**, *6*, 5635.
[92] Z. Chen, Z. Zhang, *Water Sci Technol* **2020**, *82*, 207.
[93] A. B. D. Cassie, *Discuss. Faraday Soc.* **1948**, *3*, 11.
[94] H. Wang, X. Zhao, J. Wang, Z. Wang, D. Wang, J. Tian, *Case Stud. Therm. Eng.* **2021**, *27*, 101319.
[95] A. Malli, H. R. Seyf, M. Layeghi, S. Sharifian, H. Behravesh, *Energy Convers. Manage.* **2011**, *52*, 2598.
[96] A. Geissler, F. Loyal, M. Biesalski, K. Zhang, *Cellulose* **2014**, *21*, 357.
[97] M. Stanzel, R. Brilmayer, M. Langhans, T. Meckel, A. Andrieu-Brunsen, *Microporous Mesoporous Mater.* **2019**, *282*, 29.